Acta Oceanol. Sin., 2021, Vol. 40, No. 1, P. 162–172
https://doi.org/10.1007/s13131-020-1674-1
http://www.hyxb.org.cn
E-mail: hyxbe@263.net

Alteration of estuarine circulation pattern due to channel modification in the North Passage of the Changjiang River Estuary

Lei Zhu[1, 2*], Xiaodong Chen[1], Zhimo Wu[1]

[1] School of Marine Science, Sun Yat-sen University, Guangzhou 510275, China

[2] Southern Marine Science and Engineering Guangdong Laboratory (Zhuhai), Zhuhai 519090, China

Received 23 May 2020; accepted 8 July 2020

Abstract

The exchange flow structure was examined in the North Passage of Changjiang River Estuary, where a deep waterway project (DWP) was carried out to improve the navigability. Before the construction of the DWP, the friction effect played a significant role in shaping the transverse structure of the exchange flow. The turbulent eddy viscosity generated near the seabed can be transferred to the upper water column, which facilitated vertical momentum exchange. As a result, the landward inflow extended to –2 m below the water surface and the seaward outflow was concentrated on the shallow shoal on the southern side of the cross section. After the construction of the DWP, the turbulent mixing was suppressed as a result of density stratification. The friction felt by the water was constrained in the lower half of the water column and the vertical momentum exchange was reduced. Meanwhile, the channel became dynamically narrowed with a Kelvin number of 0.52. Therefore, the Coriolis played a minor role in shaping the transverse structure of the exchange flow. As a consequence, the exchange flow featured a vertically-sheared pattern, with outflow at the surface and inflow underneath. Additionally, the gravitational circulation was enhanced due to increase in along-channel density gradient and stratification. The exchange flow components associated with the lateral processes (residual currents induced by eddy viscosity-shear covariance and lateral advective acceleration) were reduced, which suggests that lateral processes played a minor role in modifying the along-channel dynamics when the estuary becomes dynamically-narrowed.

Key words: exchange flow, stratification, lateral circulation, Changjiang River Estuary

Citation: Zhu Lei, Chen Xiaodong, Wu Zhimo. 2021. Alteration of estuarine circulation pattern due to channel modification in the North Passage of the Changjiang River Estuary. Acta Oceanologica Sinica, 40(1): 162–172, doi: 10.1007/s13131-020-1674-1

1 Introduction

Estuaries have experienced severe human intervention because of their unique geophysical locations, which caused severe geomorphological and physical changes. For example, tidal range was amplified in the West River network after a dredging project in the Zhujiang River (Pearl River) Estuary (Yuan and Zhu, 2015). The deepening of the Newark Bay has led to an enhancement in density stratification and a doubling of the exchange flow (Chant et al., 2018). The altered estuarine circulation further induced an increase in turbidity, sediment trapping, and migration of turbidity maximum zone (Winterwerp, 2011). These trapped sediments have become hinders for navigations channels and expensive dredging were carried out to maintain the navigability. In addition, large amounts of pollutants were also accumulated inside estuaries since many of them were adhere to fine sediments (Lesueur et al., 2015), which posed threatens for water quality and estuarine ecosystem (Astrahan et al., 2017). Therefore, it is necessary to understand the response of estuarine circulation to channel modification.

The Changjiang River Estuary is a typical example, which was subject to intensive morphological evolution because of construction of navigation channels and reduction of sediment load from the river catchment (Zhu et al., 2016). Wang et al. (2010) found that the water age increased for nearly 5 d near the bottom after the construction of the Deep Waterway Project (DWP). The landward circulation was found to be intensified in the North Passage due to the newly-built navigation works (Wu et al., 2010). The change in circulation further altered the sediment transport and accretion/erosion processes of the estuary. The intensive circulation resulted in sediment accumulation, which was highly contributed to the navigation siltation (Liu et al., 2011). The newly-built project obstructed the sediment exchange between channel and shoal, which induced severe deposition along the training walls (Luan et al., 2018).

Although the change in estuarine circulation induced by the engineering works has been well-studied, the mechanism that leads to such changes has not yet been fully investigated. Most studies in the North Passage still focus on the two-dimensional (longitudinal and vertical) estuarine exchange flow along the deep channel, which neglected the transverse structure of the flow pattern. Many studies have shown that the exchange flow structure in an estuary is essentially three-dimensional and the transverse variability is also important in driving the dispersion of salt and other materials. Fischer (1972) found that it is the

Foundation item: The National Natural Science Foundation of China under contract Nos 51761135021, 41576098 and 41980851; the Fundamental Research Funds for the Central University under contract No. 19LGPY96.
*Corresponding author, E-mail: zhulei28@mail.sysu.edu.cn

transverse shear acted as the dominant mechanism for dispersion. Huzzey (1988) also detected the transverse variation in density structure in York River estuary. Thus, it is necessary to consider the transverse structure of exchange flow in diagnosing estuarine dynamics. Wong (1994) employed an analytical model to detect the effect of cross-channel variation in bathymetry on the exchange flow pattern. He examined the exchange flow in a triangular basin and found that the inflow was concentrated in the channel and extended to the surface, while the outflow was restricted on the side shoals. However, the inflow spread widely in the lower layer with a flat bottom estuary. Kasai et al. (2000) further explained the exchange flow pattern was determined by friction, which is measured by the Ekman number (E_k). When friction is dominant, the exchange flow presents the same pattern as Wong's results. With small value of Ekman number, the rotating effect is prominent and the flow pattern shows a two-layer structure with inflow near the bottom and outflow on the upper layer. The ratio between basin's width and the internal Rossby deformation radius, which is expressed by the Kelvin number (*Ke*), is also important in determining the exchange flow pattern (Valle-Levinson, 2008). When an estuary is dynamically wide (*Ke*>1), the exchange flow pattern is characterized as laterally sheared with inflow in the channel and outflow over the shoals.

In addition to the gravitational circulation, the nonlinear advective acceleration associated with lateral circulation (flow that is normal to the channel orientation) has been found to be important on estuarine exchange flow. Based on the tidally averaged along-channel momentum balance in an idealized model, Lerczak and Geyer (2004) found that lateral advection acceleration is comparable to or larger than the pressure gradient force and stress divergence. Spatially, the lateral advection term acts as a seaward driving force for surface water and landward driving force for bottom water, thus, augmenting the strength of exchange flow. The modeling study in the Hudson River Estuary has shown that the nonlinear lateral advection acts in concert with the baroclinic pressure gradient force under variable forcing conditions, reinforcing the landward residual flow (Scully et al., 2009). Many studies also focused on the covariance of the tidal fluctuation of eddy viscosity and the vertical shear of velocity, which is another important driver for exchange flow (Burchard and Hetland, 2010). The covariance can be generated by peoridic mixing during a flood-ebb period (Jay and Masiak, 1994). In wide estuaries with transverse variation in bathymetry, lateral processes are more important in generating the covariance (Burchard and Schuttelaars, 2012). More recently, Dijkstra et al. (2017) proposed the concept eddy viscosity-shear covariance (ESCO) to describe the variance terms.

Previous studies of estuarine circulation in the North Passage of the Changjiang River Estuary mostly focused on the two-dimensional (longitudinal and vertical) structure. Based on *in-situ* observations, Shen et al. (1986) figured out the two-layer structure of estuarine circulation, in which barotropic force drives a seaward flow at the surface and a density-driven landward flow near the bottom. Combined with sediment settling and resuspension processes, a turbidity maximum was formed near the landward limit of saltwater intrusion (Li and Zhang, 1998). The estuarine circulation also exhibited seasonal variation in response to river discharge, with bottom landward velocity in the order of 0.05–0.10 m/s in the dry season and 0.15–0.20 m/s in the wet season (Pu et al., 2015). Many studies also examined the change in estuarine circulation due to the construction of the DWP. The estuarine circulation was found to be intensified as a result of enhanced stratification and increased longitudinal density gradient (Wang et al., 2010; Jiang et al., 2012). These studies have improved our understanding of the estuarine circulation in the North Passage and its response to channel modification. However, the transverse structure of estuarine circulation has been neglected in previous studies. The Changjiang River Estuary has a complex channel-shoal bathymetry and estuarine circulation may exhibit significant variation over a transverse section. Moreover, the transverse structure of estuarine circulation should be largely altered due to channel modification. Thereby, the objectives of this study are: (1) to investigate the transverse structure of estuarine circulation and its alteration induced by the construction of the DWP; (2) to demonstrate the behind mechanism that controls the change in estuarine circulation.

2 Study site

The Changjiang River Estuary is located along the central eastern coast of China (Fig. 1a), with a latitude ranging from 30°40′ to 31°11′N and a longitude ranging from 120°55′ to 123°00′E. The Changjiang River Estuary is a complex estuarine system with three-level bifurcation and four outlets (i.e., North Branch, North Channel, North Passage and South Passage). It is first divided into the South Branch and North Branch by the Chongming Island, and then the South Branch is divided into the South Channel and North Channel by the Changxing Island and Hengsha Island. The South Channel further branches into South Passage and North Passage with Jiuduan Shoal in the middle. The estuary receives large amounts of freshwater and sediment input from the Changjiang River. The annual river runoff and suspended sediment load between 1950–2010 are approximately 900×10^9 m^3/a and 390×10^6 t/a at Datong Station, about 640 km upstream of the river mouth, where daily discharge and sediment concentration are measured. The Changjiang River Estuary is a meso-tidal estuary, with a mean tidal range of 2.66 m at the estuary mouth. The tidal range decreases toward the upstream. Symmetric semidiurnal tides are observed outside the mouth and asymmetric tides are observed inside the mouth. Under the combined influence of a large freshwater input and tide, the tidal currents in the estuary are strong. The maximal current is greater than 3.0 m/s. The estuary is a partially mixed estuary. However, it may change to a highly stratified or mixed estuary depending on tidal ranges and river discharge (Pu et al., 2017; Shao et al., 2017).

The turbidity maximum zone, formed under the combined effects of estuarine circulation (Shen et al., 1986), sediment flocculation (Guo et al., 2017), and sediment resuspension (Li and Zhang, 1998), is located in the lower reach of the South Passage, North Passage and North Channel. The long-term sediment accumulation in the turbidity maximum zone results in a large-scale sand bar within the estuary mouth, which has a mean water depth of about 7.0 m (Chen et al., 1999). In order to improve the navigable capacity, the DWP was constructed during 1998–2010 (Fig. 1b). It consists of two along-channel training walls, nineteen groins and diversion works at the inlet. The navigation channel is about 50 km long, 350–400 m wide, and the main channel was deepened to 12.5 m. The project is divided to three stages. Phase 1 (1998–2001) involved construction of two training-walls, ten groins in the North Passage and diversion work at the inlet. During the Phase 2 (2001–2004), the training-walls were extended seaward and the groins were lengthened. Nine new groins were added and the navigation channel was dredged to 10 m. The water depth was increased to 12.5 m at the end of 2010 by local adjustment and massive dredging during the Phase 3 (2006–2010). Following the completion of the project,

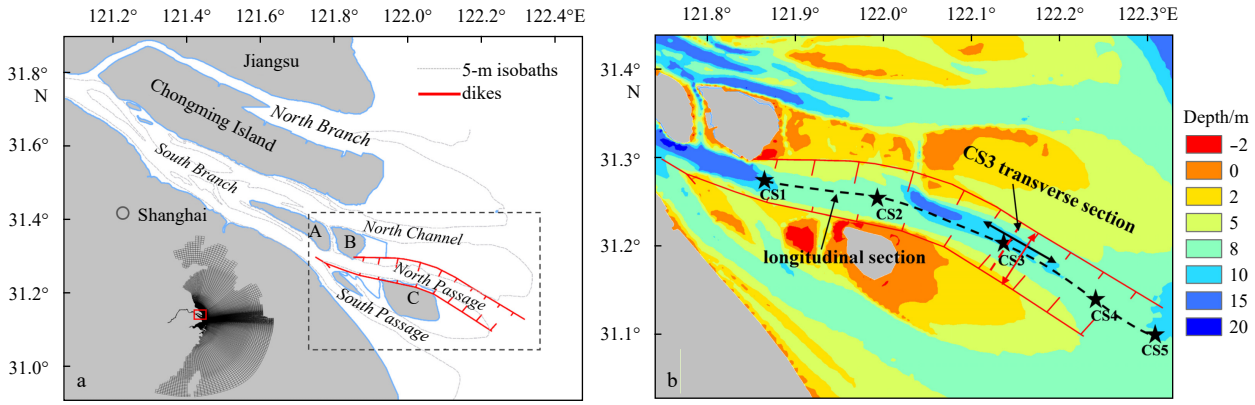

Fig. 1. Sketch of the Changjiang River Estuary and model grid (a); and bathymetry in the North Passage and its adjacent area (b). In a, A, B and C represent Changxing Island, Hengsha Island and Jiuduan Shoal, respectively. In b, black stars indicate the measurements sites, red dashed line denotes the CS3 transverse section and black dashed line denotes the longitudinal transect, the black solid and red solid arrows denote the orientations of the along-channel and lateral flows, respectively; the directions are defined as: positive landward and negative seaward in the along-channel direction, positive toward the northern dike and negative toward the southern dike in the lateral direction.

unexpected siltation occurred in the middle reach of the North Passage. The routine maintenance of the navigation channel has become a heavy burden. It is expected that the circulation processes have been altered, which will contribute to the siltation.

3 Methodology

3.1 *Numerical modeling*

The environmental fluid dynamics model (EFDC) was used in this study to investigate the hydrodynamic change in the estuary. The model solves the Navier-Stokes equation for a domain with free surface assumption. The modified Mellor and Yamada level 2.5 turbulence closure scheme was implemented in the model to obtain the vertical viscosity and diffusivity (Mellor and Yamada, 1982; Galperin et al., 1988). The model uses a structured orthogonal curvilinear grid in the horizontal and sigma coordinate in the vertical. The model resembles the widely used Blumberg-Mellor model in both the physics and the computational scheme utilized (Blumberg and Mellor, 1983).

Because of frequent water exchanges between Changjiang River Estuary and its adjacent seas, the model domain covers the Bohai Sea, Yellow Sea and East China Sea (Fig. 1a). The use of a large-domain model can also remove the errors caused by the influence of the open sea boundary. There are 25 922 cells in the horizontal plane with cell length varying from 150 m to approximately 30 000 m at the open sea boundary. Sixteen layers of water column of the same thickness using sigma coordinate were specified vertically. In order to represent the complex geometry in the estuary, the grids follow the deep channels and high-resolution grid cells are placed inside the North Passage. The upstream river boundary is located at the tidal limit of the Changjiang River Estuary, where daily river discharge is measured. Nine harmonic tidal constituents, namely M_2, S_2, N_2, K_2, O_1, K_1, P_1, M_4 and MS_4, are forced at the open sea boundary. The tidal constituents were extracted from the global tidal data from the Delft Dashboard (http://delft-dashboard.software.informer.com/). To better simulate the hydrodynamics in the shallow shoals, the wetting-drying method are switched on during the simulation. The constant salinity of 34 is used at the model open boundary since the salinity at the open boundary is primarily saline water with little influence from the freshwater. Over the model domain, the temperature is treated as a constant of 20°C as we focus inside the estuary, where the temperature contributes little to the stratification. The hydrodynamic roughness z_0, varying from 0.002 m to 0.008 m, is used in the model based on model calibration.

In order to compare the hydrodynamics prior to and after the construction of DWP, the numerical simulations are conducted for scenarios based on the bathymetries in 1997 and 2010. The multi-year (1950–2010) averaged river discharge, 29 000 m^3/s, was used at the riverine boundary. For the 2010 simulation, the training walls and groins were simulated by blocking specified faces of the grid cells. These configurations of numerical models enable us to distinguish the estuarine circulation changes caused by the DWP. For each of the scenario, the model was run for 180 d and only the results for the last 29 d were used. As this study focus on change in exchange flow pattern induced by the newly-built navigation works, model outputs of salinity and tidal current were averaged during a 29-d period to remove tidal signal (Boon, 2004) and the spring-neap variation of exchange flow was neglected. To fully investigate the changes in flow pattern, a longitudinal section, from CS1 to CS5 (Fig. 1b), and a transverse section at CS3 were selected since it locates at the core zone of the turbidity maximum and suffers heavy siltation following completion of the DWP. The longitudinal section helped exhibiting the saltwater intrusion and along-channel variation in exchange flow. The transverse section was selected to represent the changes in exchange flow pattern, lateral flows and salinity profile.

3.2 *Model calibration*

The model was validated for its capability for simulation of both tidal currents and salinity before and after the construction of the DWP. Field data of tidal current and salinity during the summer in 2000 and 2009 were collected. These two data sets can be representatives of the hydrodynamics before and after the channel modification. The measurement sites are named CS1 to CS5 and at the same locations for both 2000 and 2009. Both of the two *in-situ* measurements were conducted during spring tides and lasted for more than 25 h.

The comparisons between tidal currents and salinity between the simulated results and observations are shown in Figs 2 and 3. We evaluated the model skill quantitatively against the measured tidal current and salinity time series. The model skill score (*SS*) utilized by Allen et al. (2007) was adopted here, which is

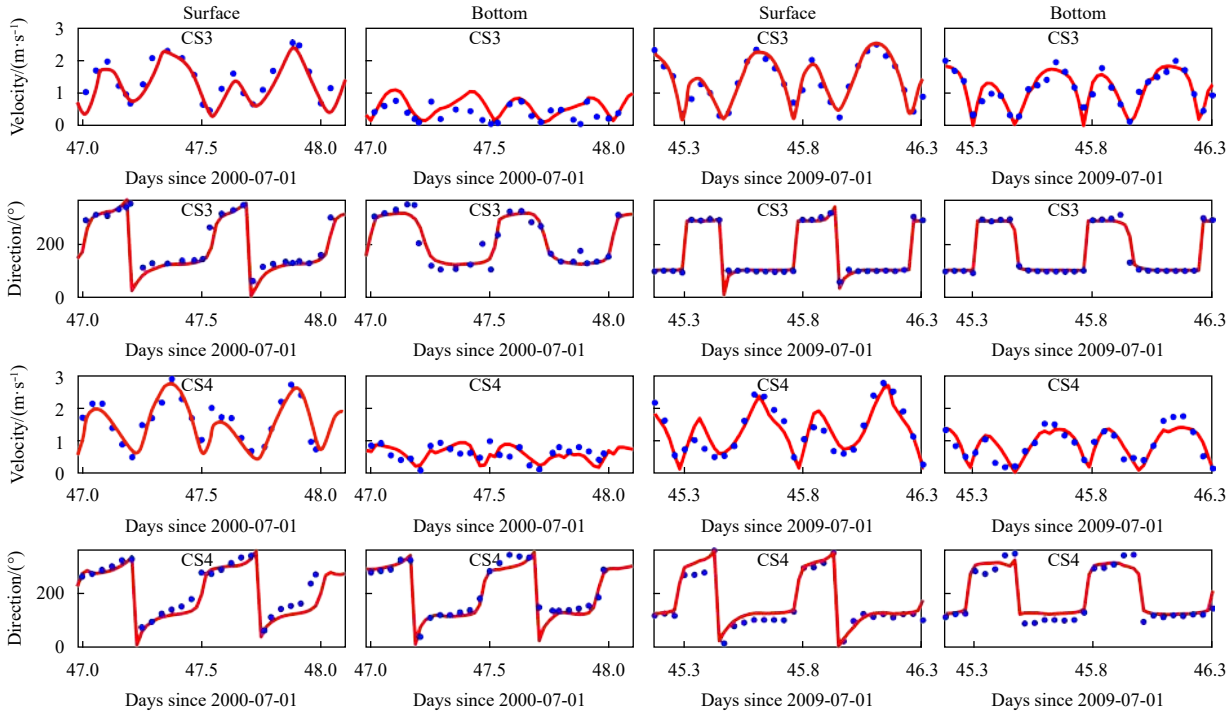

Fig. 2. Comparisons between modeled (solid lines) and observed (dots) tidal current.

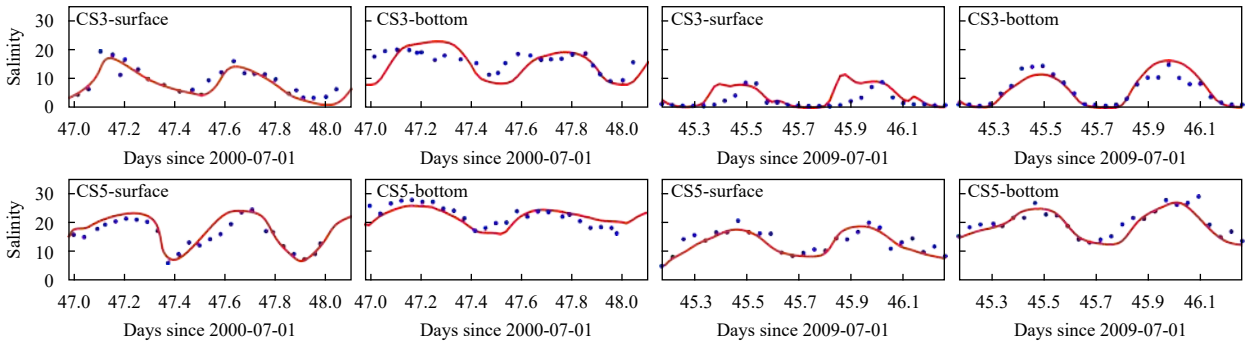

Fig. 3. Comparisons between modeled (solid line) and observed (dots) salinity.

$$SS = 1 - \frac{\sum_{i=1}^{N}(X_{\mathrm{m}} - X_{\mathrm{o}})^2}{\sum_{i=1}^{N}(X_{\mathrm{o}} - \bar{X}_{\mathrm{o}})^2}, \tag{1}$$

where X is the variables of interest and $\bar{X}$ is the time mean, m and o represent the value is modeled or observed, respectively. The skill score shows an index of model-data agreement, with a value of 1 indicating perfect agreement and a value of 0 indicating complete disagreement. Maréchal (2004) categorized an SS>0.65 as "excellent", 0.50–0.65 as "very good", 0.20–0.50 as "good", and <0.20 as "poor".

The modeled tidal currents follow the observations reasonably well for both 2000 and 2009, and the model skill scores are greater than 0.5 at most stations, which are within the score levels of "excellent" and "very good". The ebb tidal currents in 2009 were generally stronger than that observed in 2000, which may be induced by the river discharges, 35 500 m^3/s and 43 600 m^3/s for the 2000 and 2009 observations, respectively. The modeled salinity varied in almost the same range as the observed salinity within a flood-ebb tidal cycle. It is notable that the salinity difference between the surface and bottom layers was larger for the 2009 measurement, indicating that the stratification was enhanced. Some discrepancies occurred during peak flows, probably due to the complex bathymetry and the flow division between the channels (e.g., North Passage and South Passage). The skill score of salinity simulation varies from 0.52 to 0.91 and has a better skill near the bottom than the surface. Overall, the model results are acceptable and allowed us to conduct numerical simulations to diagnose the dynamics in the Changjiang River Estuary.

4 Results

4.1 *Exchange flow*

The field measurements of salinity showed that an enhancement of stratification after the construction of the DWP, which has a major influence on exchange flow (Hansen and Rattray, 1965). However, the buoyancy inputs from the upstream were not identical because the differences in river discharges. Therefore, the following investigations about the exchange flow and

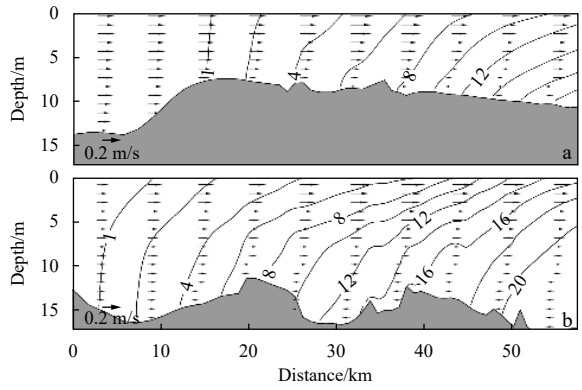

Fig. 4. Averaged salinity and residual current along the North Passage over a 29-d period in 1997 (a) and 2010 (b).

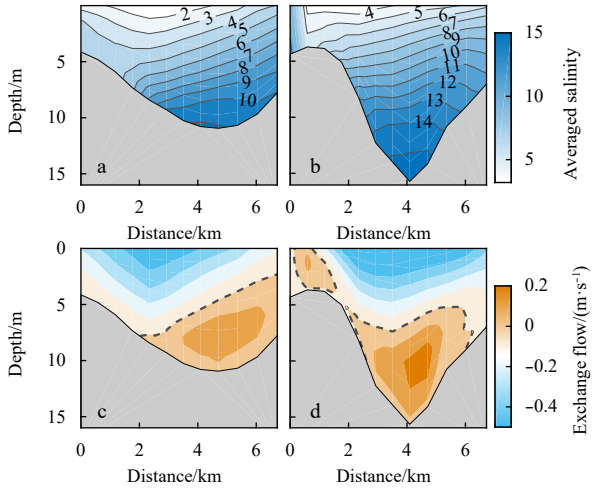

Fig. 5. Transverse structure of averaged salinity (a, b) and exchange flow (c, d; the dashed lines denotes the interface between inflow and outflow) along the CS3 section over a 29-d period in 1997 (a, c), and 2010 (b, d).

the associated driving mechanisms were mostly analyzed based on model results, which was forced by the same boundary conditions except for the bathymetry. Model simulation before the construction of the DWP showed that the freshwater/saltwater interface was located 15 km downstream of the CS1 station (Fig. 4a). The interface of freshwater/saltwater was pushed 11 km upstream after the completion of the DWP (Fig. 4b). The salinity structure for both of the two model scenarios showed a classical pattern of a partially mixed estuary, with a weak pycnocline from the surface to bottom as exhibited in the mean salinity profile (Valle-Levinson, 2010). Compared to the salinity structure prior to the DWP, a sharp salinity front, where the salinity ranged from 6 to 16, was formed following the completion of the engineering works. A two-layered exchange flow manifested in the North Passage, with inflow at the bottom and outflow at the surface. Coinciding with the changes in salinity, increase in landward residual current was most vigorous inside the salinity front. Near the surface, the seaward outflow increased by 0.1 m/s as the flow concentrated in the main channel after channel deepening.

Because of the transverse variation in bathymetry and hydrodynamics, the exchange flow may differ largely between the channel and the shoal. Here we present the transverse structure of the exchange flow at CS3 transect (Fig. 1b). The exchange flow and salinity showed that the heavier salt water intruded from the deep channel on the right (looking upstream) and low salinity was observed on the shallow part prior to the DWP (Fig. 5a). In accordance with the salinity structure, the net inflow tended to concentrate on the deep channel of the cross-section and extended to 2 m below the water surface in the northern bank (Fig. 5c). On the contrary, the net outflow concentrated on the shallow area of the left side and the inflow-outflow interface inclined to the left in accordance with the pycnocline. The exchange flow pattern featured a laterally-sheared structure as defined by Valle-Levinson (2008). After the construction of the DWP, the salinity profile was nearly flattened over the transverse section, thus the water column became more stratified (Fig. 5b). Similar to the salinity profile, the inflow was compressed in the lower half of the water column and the seaward outflow was in the upper layer (Fig. 5d). The exchange flow changed to a vertically-sheared pattern. It is notable that the inflow on the left shoal was not taken into account, since it was resulted from the sheltering effects of the groins instead of density-driven current (Ge, 2010).

4.2 *Lateral flows*

In this section, we present the change in lateral flows before and after the construction of the DWP. For the 1997 simulation, saltier water was transported upstream via the deep channel and a strong transverse salinity gradient was generated during the flood slack (Fig. 6a). The along-channel showed a baroclinic signal, with maximum current speed presenting in the middle of the water column instead of at the surface (Fig. 6e). A strong lateral shear in the along-channel was exhibited. The lateral flow was greater in magnitude than the along-channel flow because the along-channel flow was weak during flood slack. The lateral flow showed a two-layer structure with surface water flowed northward and near-bottom flow directed southward. Fresher water was advected to the right side of the channel by the northward lateral flow through the upper layer, generating distinct transverse salinity gradient. During the ebb slack, the salty water was observed on the lateral boundaries (Fig. 6b), which is caused by the rapid downstream movement of water parcel in the deep channel (Fig. 6f). The salinity variation during a flood-ebb tidal cycle indicated distinct periodic stratification, which has been proved to be induced by both the along-channel and lateral tidal straining processes (Chen et al., 2020). This suggests that the ESCO is important in driving the estuarine circulation, for which we will discuss later. The lateral flow was reduced and had a divergent structure during the ebb slack, which featured the characteristics of lateral flow driven by differential advection (Nunes and Simpson, 1985).

After the construction of the DWP, the water column was stratified with distinct salinity gradient during the flood slack (Fig. 6c). The mixing effect was constrained close to the seabed. In accordance with the salinity structure, the high-speed zone moved to the lower layer of the water column (Fig. 6g). The magnitude of lateral flow reduced over most part of the transverse section, because the water exchange between the shallow shoal and channel was largely blocked after by the newly-built training walls (Jiang et al., 2012). Surface lateral currents were convergent and bottom lateral currents were divergent. The convergence center located consistently with the maximum along-channel current, suggesting close links between longitudinal and lateral hydrodynamics. During the ebb slack, stratification was developed over the entire transverse section with a flattening salinity profile (Fig. 6d). The surface and bottom longitudinal tidal currents were out of phase and flowed in opposite directions (Fig. 6h).

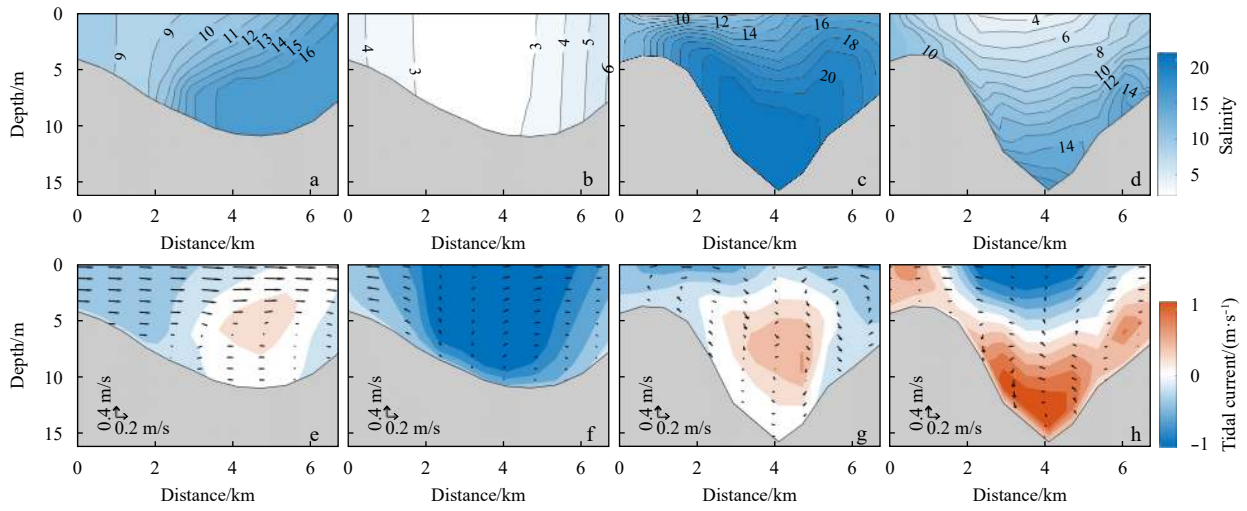

Fig. 6. Transverse distribution of salinity (a–d) and tidal current (e–h) during flood slack (a, c, e, g) and ebb slack (b, d, f, h) at the cross section of CS3 during a spring tide in 1997 (a, b, e, f); and 2010 (c, d, g, h).

The lateral flow exhibited a convergent structure similar to the simulation for 1997, however, the magnitude of lateral flow was dramatically reduced.

4.3 *Subtidal along-channel momentum balance*

The dominant force for estuarine exchange flow was assumed to be the pressure gradient force and it was balanced by stress divergence (Hansen and Rattray, 1965; Trowbridge et al., 1999; Geyer et al., 2001). However, recent studies demonstrated that the lateral advective acceleration can be another driving mechanism for exchange flow by transversely adjusted the along-channel momentum (Lerczak and Geyer, 2004; Scully et al., 2009). On subtidal time scales, the along-channel momentum balance can be expressed as:

$$\frac{1}{\rho_0}\left\langle\frac{\partial P}{\partial x}\right\rangle+\left\langle u\frac{\partial u}{\partial x}\right\rangle+\left\langle v\frac{\partial u}{\partial y}\right\rangle+\left\langle w\frac{\partial u}{\partial z}\right\rangle=-\left\langle\frac{\partial}{\partial z}\left(A_z\frac{\partial u}{\partial z}\right)\right\rangle, \tag{2}$$

where A_z is the vertical eddy viscosity; P is the pressure gradient; u, v, and w are the velocity components along the directions of x, y, and z, respectively; and ρ_0 is the water density. The angle brackets denote tidal average. The first term on the left-hand-side is the pressure gradient force, which consists of both barotropic and baroclinic components; the second term on the left hand-side is the along-channel advective acceleration; the fourth and the last term on the left-hand-side is along-channel advective acceleration; the term on the right-hand-side is stress divergence. The momentum balance at subtidal time scales is approximately steady with little contribution from the tendency term and Coriolis force, which have been neglected in Eq. (3). Because of the velocity was nearly homogeneous along the channel (Fig. 4), the magnitude of along-channel advective acceleration is far less than the lateral advective acceleration and will not be accounted in the momentum balance.

For both the simulations, the lateral advective acceleration was in comparable magnitude with the pressure gradient force and stress divergence (Fig. 7). Before the construction of the DWP, the landward pressure gradient force occupied most region of the transverse section (Fig. 7a). The stress divergence was almost acted in the opposite direction, which directed seaward in the main channel and oriented landward on the southern shallow shoal (Fig. 7b). As indicated by the lateral flow in Fig. 6e, water parcels on the left shoal was advected to the channel by the northward lateral flow during flood tide. The lateral flow became divergent and led to movement of water to the shallow regions during ebb tide. In tidal average, the lateral advective acceleration directed landward over the deeper channel areas on the right part and seaward in the left portion over the shallow shoal (Fig. 7c). After the construction of the DWP, the landward pressure gradient force was augmented because of increase in both along-channel salinity gradient and water depth (Fig. 7d). As a result of enhanced stratification, the stress divergence was constrained in the lower half of the water column (Fig. 7e). The water concentrated in the main channel led to an enhancement of seaward barotropic pressure gradient force. Therefore, both the inflow and outflow were strengthened (Fig. 5d). After the construction of the DWP, the lateral circulation featured a convergent structure during the flood tide and a divergent structure during the ebb tide. The asymmetry of lateral circulation (amplitudes of lateral circulation during the flood tide greater than that during the ebb tide) results in a landward lateral advective acceleration in the main channel. In the lower part of the water column, the lateral advective acceleration acted as a significant force that accelerates the landward residual current. Meanwhile, the seaward pressure gradient force near the surface was retarded. It is notable that the amplitude of lateral advective acceleration decreased because of reduction in both lateral flow and lateral shear of along-channel current (Fig. 6).

4.4 *Lateral dynamic balance*

In order to address the driving force of the lateral current, we implemented the lateral momentum balance over the transverse section. The transverse momentum balance is expressed as:

$$\frac{\partial v}{\partial t}+u\frac{\partial v}{\partial x}+v\frac{\partial v}{\partial y}+w\frac{\partial v}{\partial z}+fu=-g\frac{\partial \eta}{\partial y}-\frac{g}{\rho_0}\int\frac{\partial \rho}{\partial y}\partial z-\frac{\partial}{\partial z}\left(A_z\frac{\partial v}{\partial z}\right), \tag{3}$$

where f is the Coriolis parameter, g means gravitational acceleration and η is the free surface elevation. The first term on the left-hand-side is the tendency; the following three terms are advect-

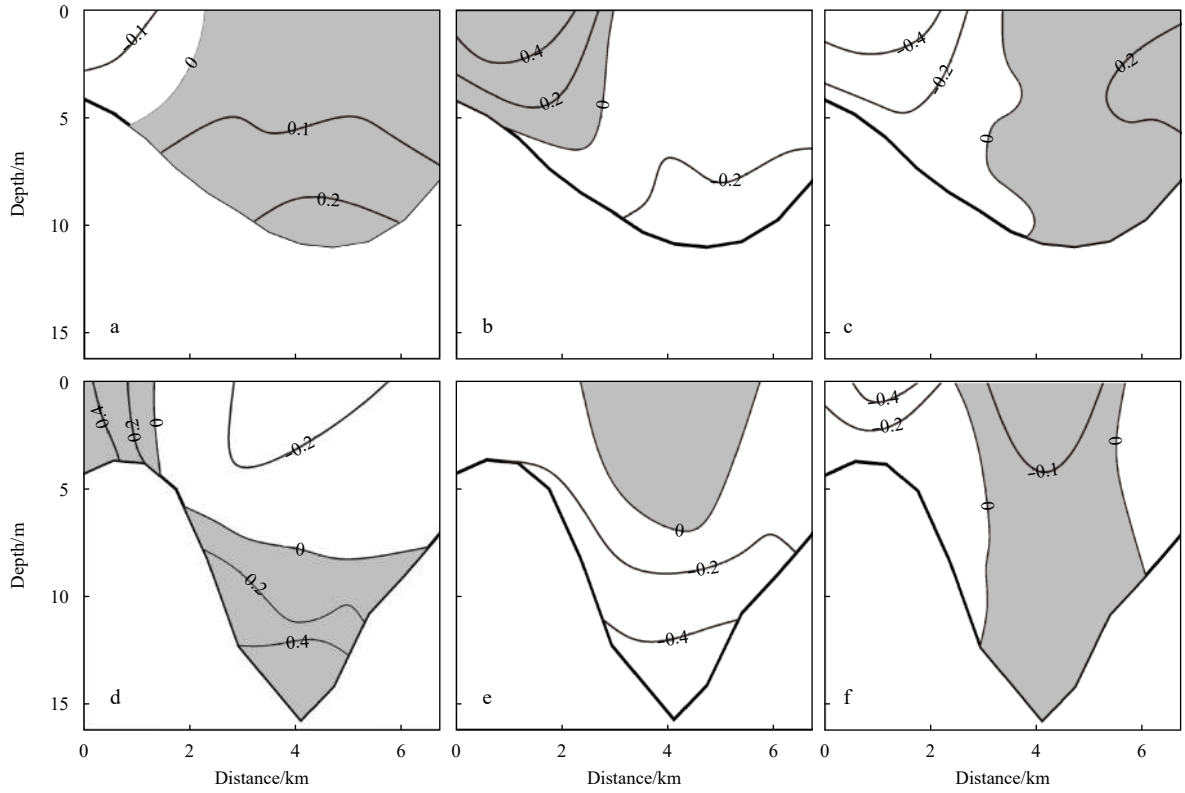

Fig. 7. The averaged along-channel momentum terms at the CS3 transverse section in 1997 (a–c) and 2010 (d–f). a and d. Pressure gradient force; b and e. stress divergence; and c and f. lateral advective acceleration $\left(\left\langle v\frac{\partial u}{\partial y}\right\rangle+\left\langle w\frac{\partial u}{\partial z}\right\rangle\right)$. The landward momentum is shaded gray and the unit is 10^{-4} m/s^2.

ive acceleration; the last term on the left-hand-side is Coriolis force. The three terms on the right-hand-side are barotropic, baroclinic pressure gradient force and stress divergence, respectively. In this study, the above acceleration terms were calculated in a cross-average sense to simplify the analysis.

In many estuaries, the lateral momentum balance was largely geostrophic with the pressure gradient forces balanced by the Coriolis forcing during most of a tidal cycle (Forrester, 1970; Li et al., 2017). In this study, the lateral momentum balance was also largely dependent on the asymmetry in bathymetry. Before the construction of the DWP, the cross-averaged baroclinic pressure gradient forces consistently directed to the south because saltier water intruded in the main channel (Fig. 8a). During the flood tide, the Coriolis force of the tidal flow dominated over the lateral pressure gradient force, which drove a strong northward lateral flow on the surface (Fig. 6e). The southward bottom lateral flow was associated with the lateral baroclinic forcing that driven by differential advection. The Coriolis force turned southward during ebb tide and has a magnitude smaller than the northward barotropic pressure gradient force. Therefore, the lateral flow directed to northward for most of the transverse sections (Fig. 6f). During the whole tidal cycle, the stress divergence term was generally stronger than the nonlinear advection and acted as a compensation to achieve momentum balance in the transverse section (Fig. 8b).

After the construction of the DWP, the asymmetry in the bathymetry was reduced. The momentum balance was still geostrophic in the first order during flood tide (Fig. 8c), which drove a convergent lateral flow near the surface and a divergent flow near the bottom in response to the changed bathymetry. The barotropic pressure gradient force was largely reduced during ebb tide as shallow shoal resides on both side of the channel. The lateral flow still featured a divergent structure and decreases in magnitude. As a result of channel deepening, the stress divergence effect decreased and the nonlinear advection contributed more in momentum balance (Fig. 8d).

5 Discussion

5.1 *Factors controlling the exchange flow structure*

The results have shown that the landward inflow was inclined to the northern side of the channel, while the seaward outflow was concentrated on the shallow shoal of the southern side before the construction of the DWP (Fig. 5c). Due to channel deepening, the inflow was constrained near the bottom and out flow was presented on the surface (Fig. 5d). In shallow coastal regions, the vertical structure of tidal velocity is ultimately determined by how the momentum from external force (e.g., barotropic or baroclinic pressure gradient force) is vertically redistributed by friction (Souza and Simpson, 1996). The friction felt by water is largely dependent on turbulent mixing, which can be largely suppressed by stratification (Geyer, 1993; Vroom et al., 2017). To quantitatively investigate the change in stratification, the buoyancy frequency was calculated:

$$N^2=-\frac{g}{\rho_0}\frac{\partial\rho}{\partial z}, \tag{4}$$

where N is the buoyancy frequency. The influence of stratification on turbulent mixing can be evaluated by Richardson num-

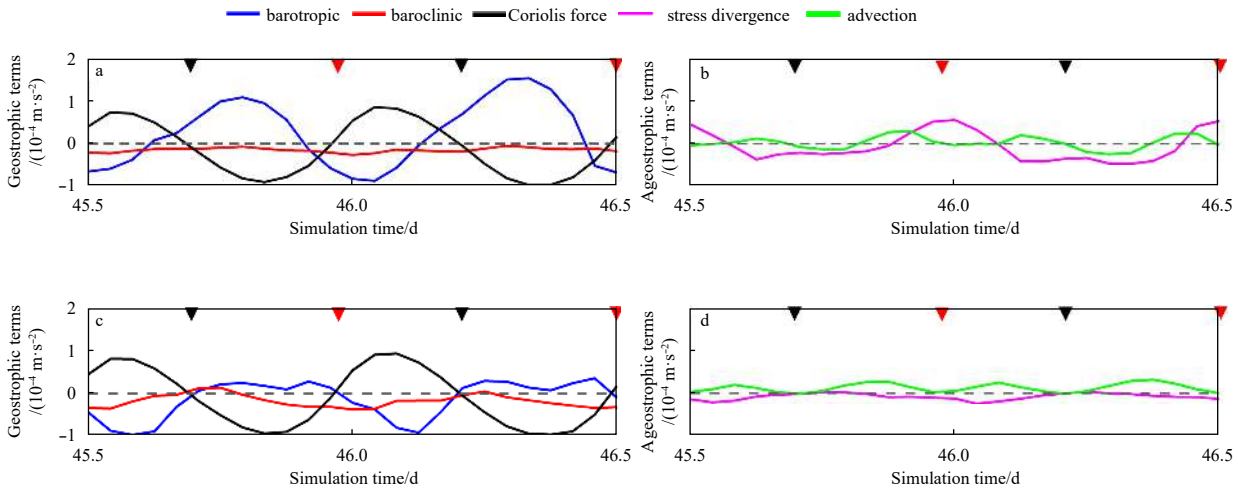

Fig. 8. Time-series of cross-averaged values of geostrophic balance terms (a. 1997; c. 2010) in the lateral momentum balance: barotropic (blue), baroclinic (red), and Coriolis force (blue), and ageostrophic terms (b. 1997; d. 2010) in the momentum balance: stress divergence (magenta), advection (green). Black and red inverted triangles in the upper axis indicate flood slack and ebb slack, respectively.

ber (*Ri*):

$$Ri = \frac{N^2}{[(\partial u/\partial z)^2 + (\partial v/\partial z)^2]}, \tag{5}$$

where $\partial u/\partial z$ and $\partial v/\partial z$ are the vertical shears in along-channel and lateral flow. The squared buoyancy and Richardson number was calculated based on the averaged salinity and subtidal velocity. The critical value for active mixing is *Ri*=0.25, since it is a necessary condition for the occurrence of shear instability.

The value of squared buoyancy frequency was typically less than 10^{-2} s^{-2} over the cross section (Fig. 9a). The stratification was vigorous in the deep channel with greater value of buoyancy frequency. After the construction of the DWP, the region with low value of buoyancy frequency was constrained close to the seabed (Fig. 9d). In consistence with the salinity profile, the squared buoyancy frequency had a value greater than 10^{-2} s^{-2} in the upper water column, suggesting that the density stratification was largely enhanced. By examining the change in *Ri*, we will show to what extent the turbulent mixing has been altered by the newly-built navigation works. Before the construction of the DWP, the value of *Ri* was greater than 0.25 in the upper part of the main channel (Fig. 9b), suggesting turbulent mixing was suppressed there (Fig. 9c). In the near-bottom region, where local production of turbulence was generated, the turbulent mixing was active and extended to the upper water column through the lateral boundaries. Turbulence was suppressed due to channel deepening because the value of *Ri* was greater than 0.25 for most portion of the transverse section (Fig. 9e). Active mixing was constrained close to the seabed and decreased for several magnitudes within 2 m (Fig. 9f). The suppressed turbulent mixing led to reduction of vertical momentum exchange, therefore, the landward inflow was constrained at the lower water column after the construction of the DWP.

Further studies pointed out that the transverse structure was determined by friction and Coriolis force. The friction impacts on exchange flow can be evaluated by Ekman number (E_k), which is defined as (Kasai et al., 2000):

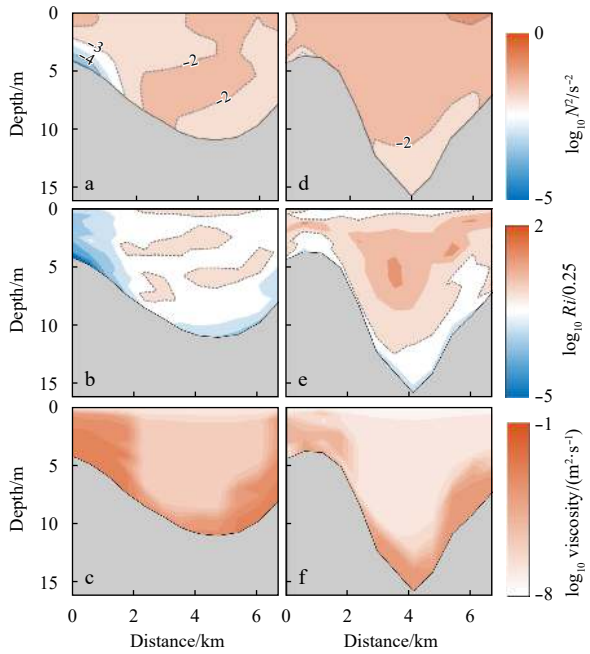

Fig. 9. Subtidal squared buoyancy frequency (a, d, shown in $\log_{10}$ scale), ratio of subtidal Richardson number to 0.25 (b, e, shown in $\log_{10}$ scale, the dashed lines denotes location where *Ri*/0.25=1) and averaged eddy viscosity (c, f, shown in $\log_{10}$ scale) during a 29-d period for the 1997 (a–c) and 2010 (d–f) simulations.

$$E_k = \frac{A_z}{fH_0^2}, \tag{6}$$

where H_0 is the maximum water depth over the transverse section. The thickness of the inflow is evaluated by the Ekman depth (*d*):

$$d = \sqrt{2E_k}H_0. \tag{7}$$

The Kelvin number (*Ke*) is ratio between basin's width with to internal Rossby deformation radius:

$$Ke = \frac{B}{R_d}, \tag{8}$$

where B is width of the channel, R_d is the internal Rossby deformation radius and $R_d = g'h/f$, where $g' = g\Delta\rho/\rho_0$ is the reduced gravity, h is the depth of the buoyant part of the exchange flow.

The value of K_e decreased from 1.21 in to 0.52, suggesting that the North Passage became dynamically narrowed after the construction of the DWP (Chen and de Swart, 2016). When Ke decreased to less than 1, the Coriolis force played a minor role in differentiating the exchange flow in the transverse section. Before the construction of the DWP, the calculated Ekman number was 0.43 and the corresponding Ekman depth was $0.93H_0$. Therefore, the landward inflow extended to the upper water column and featured a laterally-sheared pattern, with inflow in the channel and outflow over shoal, in the dynamically wide channel ($B>R_d$). The Ekman number decreased to 0.08 as the water column became stratified after the construction of the DWP. As a result, the thickness of the inflow, described by the Ekman depth, decreased to $0.4H_0$. Consequently, the salinity profile was flattened and the landward inflow was constrained in the lower layer of the water column, in consistence with the vertically-sheared exchange flow pattern described in Valle-Levinson (2008).

5.2 *Exchange flow components associated with the lateral processes*

The instantaneous salinity profile showed periodic stratification under the combined effects of tidal straining and mixing. Recent study also proposed that the lateral advective acceleration was dominant in creating vertical current shear (Burchard and Schuttelaars, 2012). It is expected that the lateral processes can be an important factor on covariance between eddy viscosity and current shear, which is important in driving the ESCO flow. Here, we calculated the ESCO flow following the method proposed by Cheng (2014) and Cheng et al. (2019). Before the construction of the DWP, the ESCO flow showed a two-layer structure, with landward flow near the bottom and seaward flow at the surface (Fig. 10a). Following the completion of the DWP, the landward ESCO flow is distinct on the shallow shoal (Fig. 10b). While in the main channel, the landward ESCO flow was constrained within a thin layer close to the seabed. The reduction in ESCO flow is mainly induced by the change in ESCO stress ($\overline{A'_z \frac{\partial u'}{\partial z}}$, where u' and A'_z are the perturbations of instantaneous along-channel velocity and eddy viscosity from the tidal mean values). The deepened channel induced permanent stratification in the upper part of the deep channel, which results in minor variation in eddy viscosity within a tidal cycle. Moreover, the decrease in lateral advective acceleration was also expected to create less variation in vertical shear (Burchard and Schuttelaars, 2012). The change in both A'_z and $\frac{\partial u'}{\partial z}$ was expected to induce a reduction in ESCO stress and the associated ESCO flow.

The model results also showed that lateral processes were also important in adjusting the momentum transversely (Fig. 7). The methods proposed by Cheng (2014) and Cheng et al. (2017) was utilized in this study to evaluate the lateral advection induced exchange flow. The lateral circulation and its associated advective processes were largely dependent on the asymmetry in bottom topography. Before the construction of the DWP, the strong northward flow led to more water parcel transporting landward via the channel on the right part of the transverse section. As a result, the lateral advective acceleration drove a landward flow in the deep part of the channel, with a maximal value of 0.05 m/s (Fig. 10c). The seaward advection-induced flow was constrained on the surface layer on the shallow shoal. After the construction of the DWP, the advection-induced exchange flow had a transverse structure that exhibited landward flow in the deep channel in the middle part of the section and seaward flow on both the shoals on norther and southern sides (Fig. 10d). The advection-induced flow was highly related the convergent structure of the lateral circulation. However, this component of exchange flow decreased in magnitude owing to reductions in both lateral flow and lateral shear of along-channel current (Fig. 6).

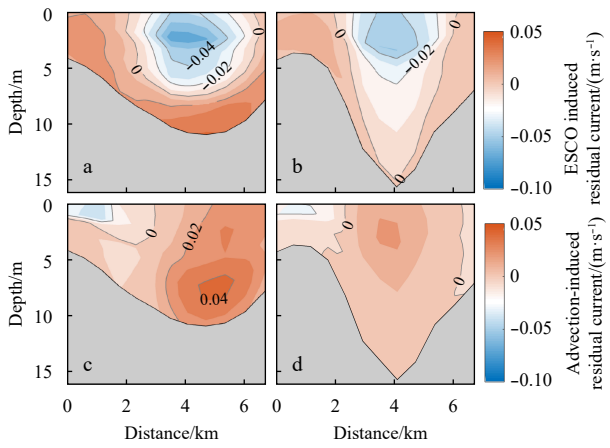

Fig. 10. The ESCO induced (a, b) and advection-induced (c, d) residual current for the 1997 (a, c) and 2010 (c, d) simulations.

These analyses suggested that the exchange flow components associated with the lateral processes have reduced after the channel narrowing. It is expected the enhanced exchange flow due to channel modification was mainly induced by the enhanced stratification and gravitational circulation, which was widely observed in other estuaries, for example, the Zhujiang River Estuary (Yuan and Zhu, 2015) and the Tampa Bay (Meyer et al., 2014). However, the estuarine exchange flow in an estuary was quite complicated and can be driven by other physical processes, such as the Stokes return flow and river-induced flow (Cheng, 2014). Therefore, a comprehensive study is merited to present each component of the exchange flow, by which an in-depth understanding of the modification of exchange flow can be obtained.

6 Conclusions

In this study, we examined the change in transverse structure of exchange flow due to navigation construction in the North Passage, Changjiang River Estuary. Both the measured salinity and model results have demonstrated that density stratification was largely enhanced after channel deepening. The turbulent mixing was suppressed by the enhanced stratification. Therefore, the vertical transfer of momentum was reduced and further modified the transverse structure of exchange flow. The landward inflow was restrained in the lower water column. The estuary became dynamically-narrow as indicated by the Kelvin number. Therefore, the Coriolis force became weak in differentiating the transverse structure of exchange flow. As a consequence, the exchange flow transferred from a laterally-sheared structure to a vertically-sheared structure. The enhanced along-channel salinity gradient and stratification resulted in a reinforcement of grav-

itational flow. By contrast, the advection-induced flow and ESCO flow was reduced after the construction of the DWP in response to the reduction in lateral advective acceleration and minor variation in periodic tidal mixing.

References

Allen J I, Somerfield P J, Gilbert F J. 2007. Quantifying uncertainty in high-resolution coupled hydrodynamic-ecosystem models. Journal of Marine Systems, 64(1–4): 3–14, doi: 10.1016/j.jmarsys.2006.02.010

Astrahan P, Silverman J, Gertner Y, et al. 2017. Spatial distribution and sources of organic matter and pollutants in the SE Mediterranean (Levantine basin) deep water sediments. Marine Pollution Bulletin, 116(1–2): 521–527, doi: 10.1016/j.marpolbul.2017.01.006

Blumberg A F, Mellor G L. 1983. Diagnostic and prognostic numerical circulation studies of the South Atlantic Bight. Journal of Geophysical Research: Oceans, 88(C8): 4579–4592, doi: 10.1029/JC088iC08p04579

Boon J D. 2004. Secrets of the Tide: Tide and Tidal Current Analysis and Applications, Storm Surges and Sea Level Trends. Chichester: Woodhead Publishing, 106–109

Burchard H, Hetland R D. 2010. Quantifying the contributions of tidal straining and gravitational circulation to residual circulation in periodically stratified tidal estuaries. Journal of Physical Oceanography, 40(6): 1243–1262, doi: 10.1175/2010JPO4270.1

Burchard H, Schuttelaars H M. 2012. Analysis of tidal straining as driver for estuarine circulation in well-mixed estuaries. Journal of Physical Oceanography, 42(2): 261–271, doi: 10.1175/JPO-D-11-0110.1

Chant R J, Sommerfield C K, Talke S A. 2018. Impact of channel deepening on tidal and gravitational circulation in a highly engineered estuarine basin. Estuaries and Coasts, 41(6): 1587–1600, doi: 10.1007/s12237-018-0379-6

Chen Wei, De Swart H E. 2016. Dynamic links between shape of the eddy viscosity profile and the vertical structure of tidal current amplitude in bays and estuaries. Ocean Dynamics, 66(3): 299–312, doi: 10.1007/s10236-015-0919-6

Chen Yu, He Qing, Shen Jian, et al. 2020. The alteration of lateral circulation under the influence of human activities in a multiple channel system, Changjiang Estuary. Estuarine, Coastal and Shelf Science, 242: 106823, doi: 10.1016/j.ecss.2020.106823

Chen Jiyu, Li Daoji, Chen Banglin, et al. 1999. The processes of dynamic sedimentation in the Changjiang Estuary. Journal of Sea Research, 41(1–2): 129–140, doi: 10.1016/S1385-1101(98)00047-1

Cheng Peng. 2014. Decomposition of residual circulation in estuaries. Journal of Atmospheric & Oceanic Technology, 31(3): 698–713

Cheng Peng, Mao Jianshan, Yu Fengling, et al. 2019. A numerical study of residual flow induced by eddy viscosity-shear covariance in a tidally energetic estuary. Estuarine, Coastal and Shelf Science, 230: 106446, doi: 10.1016/j.ecss.2019.106446

Cheng Peng, Wang Aijun, Jia Jianjun. 2017. Analytical study of lateral-circulation-induced exchange flow in tidally dominated well-mixed estuaries. Continental Shelf Research, 140: 1–10, doi: 10.1016/j.csr.2017.03.013

Dijkstra Y M, Schuttelaars H M, Burchard H. 2017. Generation of exchange flows in estuaries by tidal and gravitational eddy viscosity-shear covariance (ESCO). Journal of Geophysical Research: Oceans, 122(5): 4217–4237, doi: 10.1002/2016JC012379

Fischer H. 1972. Mass transport mechanisms in partially stratified estuaries. Journal of Fluid Mechanics, 53(4): 671–687, doi: 10.1017/S0022112072000412

Forrester W D. 1970. Geostrophic approximation in the St. Lawrence estuary. Tellus, 22(1): 53–65

Galperin B, Kantha L H, Hassid S, et al. 1988. A quasi-equilibrium turbulent energy model for geophysical flows. Journal of the Atmospheric Sciences, 45(1): 55–62, doi: 10.1175/1520-0469(1988)045<0055:AQETEM>2.0.CO;2

Ge Jianzhong. 2010. Multi-scale FVCOM model system for the East China Sea and Changjiang estuary and its applications (in Chinese)[dissertation]. Shanghai: East China Normal University

Geyer W R. 1993. The importance of suppression of turbulence by stratification on the estuarine turbidity maximum. Estuaries, 16(1): 113–125, doi: 10.2307/1352769

Geyer W R, Woodruff J D, Traykovski P. 2001. Sediment transport and trapping in the Hudson River estuary. Estuaries, 24(5): 670–679, doi: 10.2307/1352875

Guo Chao, He Qing, Guo Leicheng, et al. 2017. A study of *in-situ* sediment flocculation in the turbidity maxima of the Yangtze Estuary. Estuarine, Coastal & Shelf Science, 191: 1–9

Hansen D V, Rattray M. 1965. Gravitational circulation in straits and estuaries. Journal of Marine Research, 23: 104–122

Huzzey L M. 1988. The lateral density distribution in a partially mixed estuary. Estuarine, Coastal and Shelf Science, 26(4): 351–358, doi: 10.1016/0272-7714(88)90017-0

Jay D A, Musiak J D. 1994. Particle trapping in estuarine tidal flows. Journal of Geophysical Research: Oceans, 99(C10): 20445–20461, doi: 10.1029/94JC00971

Jiang Chenjuan, Li Jiufa, de Swart H E. 2012. Effects of navigational works on morphological changes in the bar area of the Yangtze Estuary. Geomorphology, 139–140: 205–219, doi: 10.1016/j.geomorph.2011.10.020

Kasai A, Hill A E, Fujiwara T, et al. 2000. Effect of the Earth's rotation on the circulation in regions of freshwater influence. Journal of Geophysical Research, 105(C7): 16961–16969, doi: 10.1029/2000JC900058

Lerczak J A, Geyer W R. 2004. Modeling the lateral circulation in straight, stratified estuaries. Journal of Physical Oceanography, 34(6): 1410–1428, doi: 10.1175/1520-0485(2004)034<1410:MTLCIS>2.0.CO;2

Lesueur T, Boulangé-Lecomte C, Restoux G, et al. 2015. Toxicity of sediment-bound pollutants in the Seine estuary, France, using a *Eurytemora affinis* larval bioassay. Ecotoxicology & Environmental Safety, 113: 169–175

Li Ming, Liu Wei, Chant R, et al. 2017. Flood-ebb and spring-neap variations of lateral circulation in the James River estuary. Continental Shelf Research, 148: 9–18, doi: 10.1016/j.csr.2017.09.007

Li Jiufa, Zhang Chen. 1998. Sediment resuspension and implications for turbidity maximum in the Changjiang Estuary. Marine Geology, 148(3–4): 117–224, doi: 10.1016/S0025-3227(98)00003-6

Liu Gaofeng, Zhu Jianrong, Wang Yuanye, et al. 2011. Tripod measured residual currents and sediment flux: Impacts on the silting of the Deepwater Navigation Channel in the Changjiang Estuary. Estuarine, Coastal and Shelf Science, 93(3): 192–201, doi: 10.1016/j.ecss.2010.08.008

Luan Hualong, Ding Pingxing, Wang Zhengbing, et al. 2018. Morphodynamic impacts of large-scale engineering projects in the Yangtze River delta. Coastal Engineering, 141: 1–11, doi: 10.1016/j.coastaleng.2018.08.013

Maréchal D. 2004. A Soil-based Approach to Rainfall-runoff Modelling in Ungauged Catchments for England and Wales [dissertation]. Cranfield, UK: Cranfield University

Mellor G L, Yamada T. 1982. Development of a turbulence closure model for geophysical fluid problems. Reviews of Geophysics, 20(4): 851–875, doi: 10.1029/RG020i004p00851

Meyers S D, Linville A J, Luther M E. 2014. Alteration of residual circulation due to large-scale infrastructure in a coastal plain estuary. Estuaries & Coasts, 37(2): 493–507

Nunes R A, Simpson J H. 1985. Axial convergence in a well-mixed estuary. Estuarine, Coastal and Shelf Science, 20(5): 637–649, doi: 10.1016/0272-7714(85)90112-X

Pu Xiang, Shi J Z, Hu Guodong, et al. 2015. Circulation and mixing along the north passage in the Changjiang River Estuary, China. Journal of Marine Systems, 148: 213–235, doi: 10.1016/j.jmarsys.2015.03.009

Pu Xiang, Shi J Z, Hu Guodong. 2017. The effect of stratification on the vertical structure of the tidal ellipse in the Changjiang River Estuary, China. Journal of Hydro-Environment Research, 15: 75–94, doi: 10.1016/j.jher.2017.03.004

Scully M E, Geyer W R, Lerczak J A. 2009. The influence of lateral advection on the residual estuarine circulation: A numerical modeling study of the Hudson River Estuary. Journal of Physical Oceanography, 39(1): 107–124, doi: 10.1175/2008JPO3952.1

Shao Yuyang, Shen Xiaoteng, Maa J P Y, et al. 2017. Simulating high ebb currents in the north passage of the Yangtze estuary using a vertical 1-D model. Estuarine, Coastal & Shelf Science, 196: 399–410

Shen Huanting, Zhu Huifang, Mao Zhichang. 1986. Circulation of the Changjiang River Estuary and its effect on the transport of suspended sediment. Oceanologia et Limnologia Sinica (in Chinese), 17(1): 26–35

Souza A J, Simpson J H. 1996. The modification of tidal ellipses by stratification in the Rhine ROFI. Continental Shelf Research, 16(8): 997–1007, doi: 10.1016/0278-4343(95)00042-9

Trowbridge J H, Geyer W R, Bowen M M, et al. 1999. Near-bottom turbulence measurements in a partially mixed estuary: turbulent energy balance, velocity structure, and along-channel momentum balance. Journal of Physical Oceanography, 29(12): 3056–3072, doi: 10.1175/1520-0485(1999)029<3056:NBTMIA>2.0.CO;2

Valle-Levinson A. 2008. Density-driven exchange flow in terms of the Kelvin and Ekman numbers. Journal of Geophysical Research, 113: C04001

Valle-Levinson A. 2010. Definition and classification of estuaries. In: Contemporary Issues in Estuarine Physics. New York: Cambridge University Press, 1–11

Vroom J, van der Wegen M, Martyr-Koller R C, et al. 2017. What determines water temperature dynamics in the San Francisco bay-delta system?. Water Resources Research, 53(11): 9901–9921, doi: 10.1002/2016WR020062

Wang Ya, Shen Jian, He Qing. 2010. A numerical model study of the transport timescale and change of estuarine circulation due to waterway constructions in the Changjiang Estuary, China. Journal of Marine Systems, 82(3): 154–170, doi: 10.1016/j.jmarsys.2010.04.012

Winterwerp J C. 2011. Fine sediment transport by tidal asymmetry in the high-concentrated ems river: indications for a regime shift in response to channel deepening. Ocean Dynamics, 61(2–3): 203–215, doi: 10.1007/s10236-010-0332-0

Wong K C. 1994. On the nature of transverse variability in a coastal plain estuary. Journal of Geophysical Research, 99(C7): 14209–14222, doi: 10.1029/94JC00861

Wu Hui, Zhu Jianrong, Choi B H. 2010. Links between saltwater intrusion and subtidal circulation in the Changjiang Estuary: A model-guided study. Continental Shelf Research, 30(17): 1891–1905, doi: 10.1016/j.csr.2010.09.001

Yuan Rui, Zhu Jianrong. 2015. The effects of dredging on tidal range and saltwater intrusion in the Pearl River estuary. Journal of Coastal Research, 31(6): 1357–1362

Zhu Lei, He Qing, Shen Jian, et al. 2016. The influence of human activities on morphodynamics and alteration of sediment source and sink in the Changjiang Estuary. Geomorphology, 273: 52–62, doi: 10.1016/j.geomorph.2016.07.025